

INFLUENCE OF EXTERNAL TURBULENCE ON AIRFOIL PERFORMANCE

Fernando Diogo de Carvalho Grossi, fernandogrossi@yahoo.com

Marcelo Guedes Azevedo Viana, marceloguedes@ufmg.br

Escola de Engenharia, Universidade Federal de Minas Gerais - UFMG
Curso de Graduação em Engenharia Mecânica
Av. Antônio Carlos, 6627, 31270-901, Belo Horizonte, MG, Brazil

Marcos Vinicius Bortolus, bortolus@ufmg.br

Escola de Engenharia, Universidade Federal de Minas Gerais - UFMG
Departamento de Engenharia Mecânica
Av. Antônio Carlos, 6627, 31270-901, Belo Horizonte, MG, Brazil

Abstract. *Airfoil performance can be considerably affected by atmospheric turbulence, a common phenomenon found in aircraft and wind turbines operation. Disparities between the airfoils behavior and their lift and drag polar curves obtained by means of wind tunnel testing can be identified through their entire range of operation from low angles of attack up to the nonlinear region, where the largest dependencies of the aerodynamics coefficients on the free stream turbulence level are observed. This paper analyzes the airfoils responses when submitted to different values of freestream turbulence intensity and Reynolds number, using a numerical approach based on the Finite Volume Method. Special attention is paid to the choice of an appropriate turbulence model in order to represent properly the aerodynamic flows, typically characterized by the presence of strong adverse pressure gradients and high Reynolds numbers, as well as to the mesh generation and testing. The relation between airfoils sensibilities to the external turbulence is investigated for two classical sections and is expressed by lift and drag polar curves.*

Keywords: *airfoil performance, external turbulence, finite volume method*

1. INTRODUCTION

Turbulence is an extremely complex and interesting physical phenomenon present in most of engineering application flows of which some effects are frequently unknown or ignored by researchers and engineers. A particular example is the atmospheric turbulence which can alter the performance of airplane wings and helicopter or wind turbine blades.

The purpose of this paper is to make a judicious investigation by means of numeric simulation to evaluate the variations in the performance of standard airfoils when submitted to different conditions of external turbulence. A commercial code based on the Finite Volume Method is used to solve the Reynolds-Averaged Navier-Stokes equation (RANS) with an appropriate turbulence model for aerodynamic applications available in the software, the SST (Shear Stress Transport) model. The external turbulence is numerically set through the freestream turbulence intensity and the simulations are performed for two classic NACA wing sections. The airfoils sensibilities to external turbulence are measured by means of the aerodynamic coefficients of lift and drag.

The paper is divided two parts. First, a theoretical review of some important aspects of fluid dynamics and turbulence modeling for aerodynamics is given, as well as a detailed description of the SST model. The remaining sections describe the methodology adopted and present the results obtained during the simulations, with a proper discussion and the conclusions taken.

2. TURBULENCE IN AERODYNAMICS

Turbulence occurs virtually for all aerodynamic flows of engineering interest and is mainly characterized by random variations in time of flow properties due to an increase in the transversal flux of momentum. In aerodynamics, these variations can change dramatically the forces acting on bodies immersed in the flow and cannot be neglected.

One of the several approaches to deal with turbulence is the decomposition of the flow properties into two parts, a mean component and a fluctuation. Equation 1 shows the decomposition of an arbitrary propriety ϕ .

$$\phi = \bar{\phi} + \phi' \quad (1)$$

The upper bar denotes the mean component and the prime the fluctuation. For an incompressible steady state flow with no heat transfer Equation 1 is applied only to the velocity components and the pressure. For turbulent compressible flows, the fluctuations of density and temperature must be considered (Schlichting, 2000).

For the incompressible steady state case, when the decomposed forms of the flow properties are inserted into the Navier-Stokes equations, the Reynolds-averaged Navier-Stokes (RANS) equations are obtained. Equations 2 and 3 show the RANS momentum equations for x and y .

$$\rho \left(\bar{u} \frac{\partial \bar{u}}{\partial x} + \bar{v} \frac{\partial \bar{u}}{\partial y} + \bar{w} \frac{\partial \bar{u}}{\partial z} \right) = -\frac{\partial \bar{p}}{\partial x} + \frac{\partial}{\partial x} \left[2\mu \left(\frac{\partial \bar{u}}{\partial x} \right) \right] + \frac{\partial}{\partial y} \left[\mu \left(\frac{\partial \bar{u}}{\partial y} + \frac{\partial \bar{v}}{\partial x} \right) \right] \quad (2)$$

$$+ \frac{\partial}{\partial z} \left[\mu \left(\frac{\partial \bar{u}}{\partial z} + \frac{\partial \bar{w}}{\partial x} \right) \right] - \rho \left(\frac{\partial \overline{u'^2}}{\partial x} + \frac{\partial \overline{u'v'}}{\partial y} + \frac{\partial \overline{u'w'}}{\partial z} \right)$$

$$\rho \left(\bar{u} \frac{\partial \bar{v}}{\partial x} + \bar{v} \frac{\partial \bar{v}}{\partial y} + \bar{w} \frac{\partial \bar{v}}{\partial z} \right) = -\frac{\partial \bar{p}}{\partial y} + \frac{\partial}{\partial y} \left[2\mu \left(\frac{\partial \bar{v}}{\partial y} \right) \right] + \frac{\partial}{\partial x} \left[\mu \left(\frac{\partial \bar{u}}{\partial y} + \frac{\partial \bar{v}}{\partial x} \right) \right] \quad (3)$$

$$+ \frac{\partial}{\partial z} \left[\mu \left(\frac{\partial \bar{v}}{\partial z} + \frac{\partial \bar{w}}{\partial y} \right) \right] - \rho \left(\frac{\partial \overline{u'v'}}{\partial x} + \frac{\partial \overline{v'^2}}{\partial y} + \frac{\partial \overline{v'w'}}{\partial z} \right)$$

The fluctuating components of velocity cause an apparent increase in the fluid viscosity by means of extra shear stresses (the last terms in equations 2 and 3). Thus, the fluctuations are new unknowns and define the so called closure problem, requiring some additional relations in order to solve the complete system of equations: the turbulence models. Most turbulence models used for aerodynamic flows are based on the RANS equations due to their low computational cost and considerably accurate results.

Many models frequently used in industry are based on the eddy viscosity concept, first proposed by Joseph Boussinesq in 1872 as an analogy to the Newton's law of viscosity (Schlichting, 2000). The apparent stresses are related to mean velocity gradients by the eddy viscosity μ_t (also called apparent viscosity) which becomes the new unknown to be evaluated. Equation 4 is an example of the Boussinesq's formulation for the xy turbulent stress.

$$\tau'_{xy} = -\rho \overline{u'v'} = \mu_t \left(\frac{\partial \bar{u}}{\partial y} + \frac{\partial \bar{v}}{\partial x} \right) \quad (4)$$

In order to calculate the eddy viscosity several methods were proposed, being frequently classified by the number of differential equations they use. Some models based on the eddy viscosity designed for aerodynamic applications are the Baldwin-Lomax (zero-equation model), Spalart-Allmaras (one-equation model) and the SST (two-equation model).

Two-equation models are the most used for engineering applications and usually present one algebraic equation beside of the two differential equations, which describe the transport of turbulent quantities. It should be noted that these models consider the turbulence as being isentropic. Among the two-equation models are the $k-\epsilon$, $k-\omega$ and the $k-\tau$ models. The simulations in this paper used the SST model, which is detailed in the next section.

3. THE SST MODEL

3.1 Model Description

The choice of a turbulence model should be made based on the model's suitability to the flow characteristics. In this paper the SST (Shear Stress Transport) model is used to deal with the turbulent flows over airfoils. Such flows are essentially characterized by high Reynolds numbers and strong adverse pressure gradients and require a specific turbulence modeling for their accurate prediction.

The SST model was proposed by Florian Menter in 1994, unsatisfied with the limitation of the standard eddy viscosity models in the correct prediction of boundary layer separation. Menter was concerned with aerodynamics applications and the SST was developed using an empiric approach supported by many well-documented and careful experiments. The model can be considered as an evolution of Menter's previous model, the BSL (baseline model). The BSL combines the best features of Wilcox's $k-\omega$ model and of a standard high Reynolds formulation of the $k-\epsilon$. The $k-\omega$ is used within the boundary layer, in the viscous sublayer and logarithmic regions in order to improve the computation of adverse pressure gradients and compressible flows.

A smooth transition leads to the $k-\epsilon$ model as the distance from the wall increases. The $k-\epsilon$ is also used when separation occurs and for free shear zones, avoiding the undesirable $k-\omega$ dependency on freestream values of ω , for which a small change can make the eddy viscosity vary up to 100% for those regions (Menter, 1992). The SST follows the same approach and indeed uses the same blending function as the BSL for the transition between the two models. The innovation is a modification in the eddy viscosity formulation which takes into account the transport of the principal turbulent shear stress. No damping functions are needed as the $k-\omega$ model is employed within the viscous sublayer. However, the model fails to a realistic prediction of the turbulence asymptotic behavior approaching to the

wall, what should not affect the computation of the friction coefficient as in the limit of wall proximity the eddy viscosity is very small compared to the molecular viscosity, thus the mean profile remains independent on the turbulence asymptotic behavior (Menter, 1994).

3.2 Mathematical formulation

In the SST, the original transport equations from Wilcox's k - ω model are multiplied by a blending function F_1 . The standard k - ε model is transformed into a k - ω formulation and the equations obtained are multiplied by $(1 - F_1)$. Thus, adding the two pairs of equations for k and ω leads to the SST transport equations:

$$\frac{\partial \rho k}{\partial t} + \frac{\partial \rho k u_i}{\partial x_i} = \tau_{ij} \frac{\partial u_i}{\partial x_j} - \beta^* \rho \omega k + \frac{\partial}{\partial x_j} \left[(\mu + \sigma_k \mu_t) \frac{\partial k}{\partial x_j} \right] \quad (5)$$

$$\frac{\partial \rho \omega}{\partial t} + \frac{\partial \rho \omega u_i}{\partial x_i} = \frac{\gamma}{\nu_t} \tau_{ij} \frac{\partial u_i}{\partial x_j} - \beta \rho \omega^2 + \frac{\partial}{\partial x_j} \left[(\mu + \sigma_\omega \mu_t) \frac{\partial \omega}{\partial x_j} \right] + 2\rho(1 - F_1)\sigma_{\omega 2} \frac{1}{\omega} \frac{\partial k}{\partial x_j} \frac{\partial \omega}{\partial x_j} \quad (6)$$

The last term in Equation 6 appears after the k - ε transformation and is called cross-diffusion. Within the viscous sublayer and logarithmic portion the blending function F_1 assumes the value of one, making a smooth transition down to zero as the distance from the wall increases, then combining the two models. F_1 is defined as follows:

$$F_1 = \tanh(\arg_1^4) \quad (7)$$

$$\arg_1 = \min \left[\max \left(\frac{\sqrt{k}}{0,09\omega y}, \frac{500\nu}{y^2\omega} \right), \frac{4\rho\sigma_{\omega 2}k}{CD_{k\omega}y^2} \right] \quad (8)$$

$$CD_{k\omega} = \max \left(2\rho\sigma_{\omega 2} \frac{1}{\omega} \frac{\partial k}{\partial x_i} \frac{\partial \omega}{\partial x_j}, 10^{-20} \right) \quad (9)$$

In order to include the transport of the principal turbulent shear stress the eddy viscosity is redefined as:

$$\nu_t = \frac{a_1 k}{\max(a_1 \omega, \Omega F_2)} \quad (10)$$

In Equation 10, F_2 is another transition function that has the value of one within the boundary layer and zero for free shear layers. In a boundary layer with adverse pressure gradients the production of k is more important than its dissipation and Bradshaw's hypothesis is verified, namely the eddy viscosity is proportional to the turbulent kinetic energy. For all other regions the standard formulation holds and ν_t is proportional to the square of k (as $\beta^* k \omega = \varepsilon$). F_2 is computed by:

$$F_2 = \tanh(\arg_2^2) \quad (11)$$

$$\arg_2 = \max \left(2 \frac{\sqrt{k}}{0,09\omega y}, \frac{500\nu}{y^2\omega} \right) \quad (12)$$

Calling ϕ_1 any coefficient from the original k - ω model and ϕ_2 the correspondent one for the transformed k - ε , the SST coefficient ϕ is calculated by a weighted sum which uses the blending function F_1 as the factor of relevance:

$$\phi = F_1 \phi_1 + (1 - F_1) \phi_2 \quad (13)$$

After Menter (1994), the improvements verified in SST global performance and in its dependency on freestream values of ω are ensured by the employ of functions F_1 and F_2 and by the computation of the additional cross-diffusion term in Equation 6. For a more detailed discussion about the SST model and for the $k-\omega$ and the transformed $k-\epsilon$ constants values the reader should view Menter's 1994 paper (see References).

4. METHODOLOGY

The aerodynamic flows studied in this work represent a great simulation challenge. Beside of complex geometries, the viscous phenomena play a fundamental role in the determination of the aerodynamic forces acting on the airfoils, thus requiring very detailed meshes and a mathematical formulation able to represent all the physics involved, namely the Reynolds Averaged Navier-Stokes equations and an appropriate turbulence model. Considering all these difficulties, the authors decided to use the Ansys CFX software for all simulations and the Ansys Mesh for meshing. Among the turbulence models available in CFX figures the SST, described previously.

4.1. Domain definition

Sizing the flow domain for external flow simulations is a quite difficult task. The domain boundaries must be distant enough from the bodies to ensure that the solution is not induced by their proximity. There is no general rule for a correct sizing, since many flow and geometric parameters can be influent, as the Reynolds and Mach numbers and the airfoil's section and angle of attack. In addition, 2D and 3D cases require, in general, different distances from the boundaries to the body and all examples found in literature can be simply considered as being rules of thumb.

For the calculations, the flow domain is initially established as a 10-meter upstream semicircle centered at the leading edge of a 1-meter chord length airfoil, followed downstream by two 25-meter upper and lower boundaries to ensure wake development and dissipation (see Figure 1). The thickness is 0.1 meter. This domain is used for meshing and, after the mesh test; a domain reduction procedure is performed as described in section 4.3 in order to minimize the computational costs. By comparison, the mesh used by Rezende *et al* (2008) in the simulation of the flow over a flat plate at 5° incidence with a Reynolds of 2.13×10^5 was a rectangle with 4 plate lengths upstream and 14 downstream the plate's leading edge.

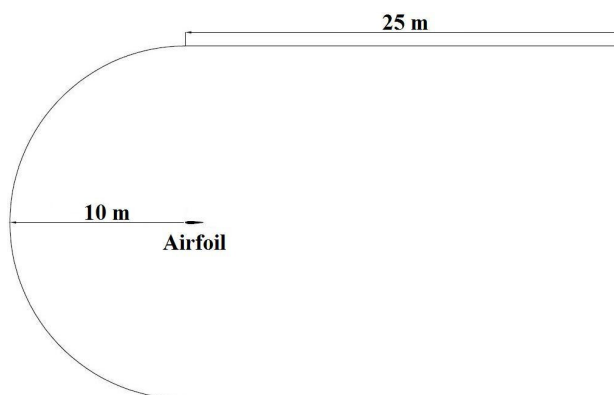


Figure 1. Initial Domain.

4.2. Meshing strategy

One critical point to any numerical simulation is the mesh generation. Again, each problem presents specific geometry and flow characteristics and there is no general rule to be followed. Each airfoil at a determined angle of attack with a specific Reynolds and freestream turbulence intensity defines a particular case for which a special mesh should be constructed and tested. Due to the very high time cost of this approach the authors opted to the creation of a strategically refined mesh that could be used in all cases.

Considering the flow over airfoils there are some relevant observations that should be kept in mind during the meshing process:

1. On the leading ledge the flow is highly accelerated, thus generating strong pressure gradients which are primarily responsible for the airfoil lift.
2. The boundary layer evolution is of extreme importance due to the nonlinear phenomena implications on aerodynamic coefficients. Therefore, the transition and separation points should be determined accurately.
3. The viscous wake must be sufficiently detailed as it influences the boundary layer evolution and consequently the forces acting on the airfoils.

Each observation defines regions in the flow that need special treatment, using appropriated refinement levels and employing specific control volume structures. For a quality mesh, smooth transitions must exist between adjacent regions and elements should not present a high aspect ratio.

Based on the above discussion, the mesh used in this paper presents specific refinement regions for the boundary layer, the leading edge, two wake levels and three transition zones from the airfoil to the boundaries (Figure 2). The wake angle was adapted to capture the flow separation at high incidences. All regions can be independently treated in Ansys Mesh, thus providing a lighter mesh and reducing the computational costs.

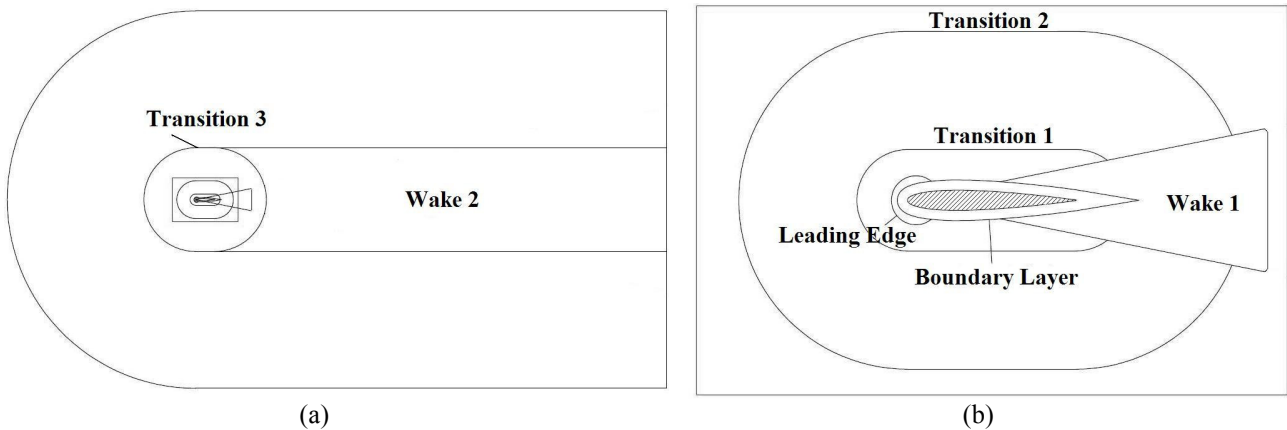


Figure 2. Mesh refinement regions in (a) global view and (b) near the airfoil.

4.3. Mesh test and domain reduction

A mesh test is performed in order to obtain a mesh-independent numeric solution. In general, Ansys CFX uses 3D unstructured grid which is transformed, in the 2D case, in triangular and rectangular prismatic control volumes. For the boundary layer region, rectangular elements are used while all the other regions use triangular control volumes. A rough mesh is initially employed, and the subsequent meshes are obtained from successive refinements of all regions, always conserving good elements aspect ratio and smooth transitions between regions. The tests were performed for the NACA 0012 section at 14° incidence, thus with important nonlinear effects. The Reynolds number was of 3×10^6 with a uniform freestream, and the convergence was based on the resultant aerodynamic force acting on the airfoil, reached by means of the independent convergences of both drag and lift coefficients. The results are shown in Figure 3 and Table 1.

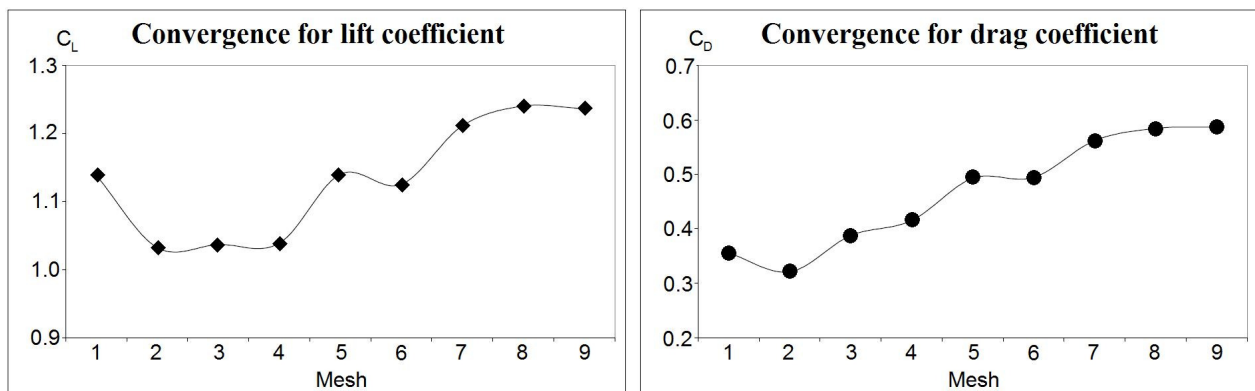


Figure 3. Convergence for lift and drag coefficients.

Table 1. Mesh test results.

Mesh	1	2	3	4	5	6	7	8	9
c_L	1.14	1.03	1.04	1.04	1.14	1.13	1.21	1.24	1.24
c_D	0.335	0.321	0.387	0.415	0.493	0.494	0.562	0.584	0.587
Δc_L (%)	-	-9.3	0.4	0.2	9.8	-1.3	7.6	2.4	-0.3
Δc_D (%)	-	-9.7	20.7	7.2	18.7	0.3	13.7	4.0	0.5

Mesh 8 was chosen for all simulations as it presented variations lower than one percent to the finer mesh for both coefficients. Figure 4 shows a preview of the final mesh near the airfoil.

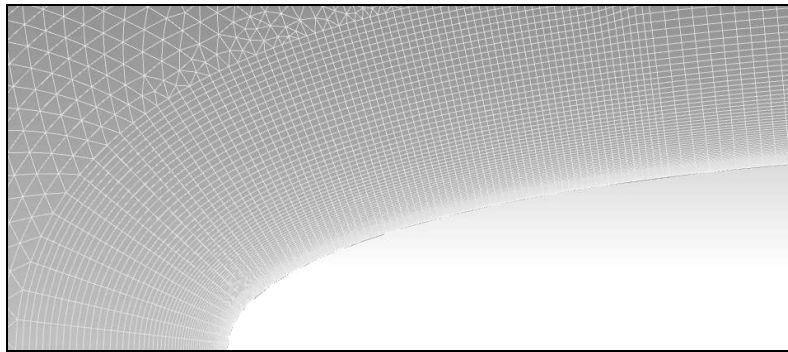


Figure 4. Final mesh near the airfoil.

The next step was the domain reduction procedure which was performed in two parts. The results are presented in Table 2. Starting from the initial domain, namely the 10-meter semicircle followed by a 25-meter rectangle, a progressive reduction of the semicircle radius was tried for domains 2 to 7. As one can see, no significant changes in coefficients values were observed. Then, the domain length was reduced through numbers 8 to 11 and the same behavior was noticed. Therefore, the definitive domain chosen for all the simulations was a 5-meter semicircle followed by an 18-meter length rectangle.

Table 2. Domain reduction results.

Domain	1	2	3	4	5	6	7	8	9	10	11
Radius (m)	10	9	8	7	6	5	4	5	5	5	5
Length (m)	25	25	25	25	25	25	25	22	20	18	16
c_L	1.24	1.25	1.25	1.26	1.24	1.26	1.25	1.25	1.25	1.25	1.25
c_D	0.584	0.589	0.590	0.598	0.597	0.586	0.590	0.589	0.587	0.587	0.590

4.4. Simulation definitions

Series of numeric simulations were performed for two standard NACA airfoils: the 0012, a symmetric and exhaustively documented section and the 23015, often used in wind turbines and general aeronautic applications. Both airfoils were evaluated from the linear portion to the stalling region, submitted to freestream turbulence intensities that go from zero up to 20%. These values cover the range of typical low-altitude atmospheric turbulence.

The Ansys CFX numerical approach consists on an implicit pressure-based algorithm which solves a transformed continuity and the momentum equations as well as the SST model equations. Heat transfer was not considered due to the low Mach number involved. The fluid model was air at 25° at sea level and the computations stopped when a residual of 10^{-5} was reached for both continuity and momentum equations. The boundary conditions set in the software are showed in Figure 5. For the inlet, the x and y components of velocity were entered, as well as the freestream turbulence intensity, thus defining the angle of attack and the Reynolds number. The z component of velocity was set to zero. In order to avoid flow confinement, the upper and lower boundaries are set as openings with freestream turbulent intensity. For the outlet, only the static pressure was assigned and set as being equal to the inlet reference pressure. The airfoil was defined as a solid wall where the no-slip condition holds, and the x - y plane boundaries were set as symmetry planes, thus establishing the two-dimensional flow.

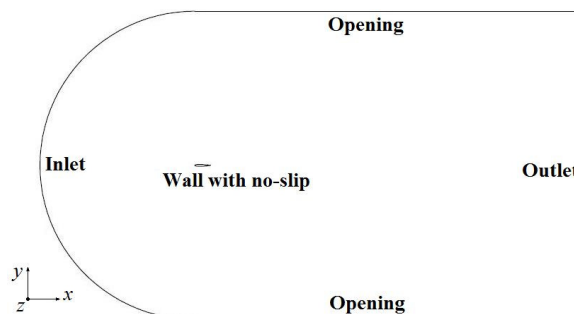


Figure 5. Boundary conditions.

The last parameter to be set was the Reynolds number, here defined based on the airfoil chord length and the freestream flow velocity. For some possible aerodynamic applications the Reynolds are on the order of 10^5 to 10^7 as shown in Figure 6, and therefore a preliminary investigation of the behavior of aerodynamic coefficients with freestream turbulence intensity was performed for these cited values and all the following simulations were done with a Reynolds number chosen among them. The results will be presented in the next section.

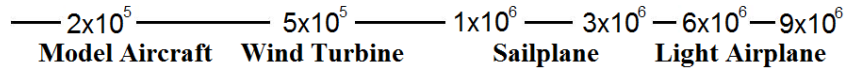


Figure 6. Reynolds number for some aerodynamic applications.

5. RESULTS

5.1. Dependency on Reynolds number

The Reynolds number test was performed for the above Re values with freestream turbulence intensities of zero and 20%. The geometry was a NACA 23015 airfoil at 16° , in order to obtain a flow in the nonlinear region which is strongly dependent on the viscous phenomena. Figure 7 presents the plots for lift and drag coefficients.

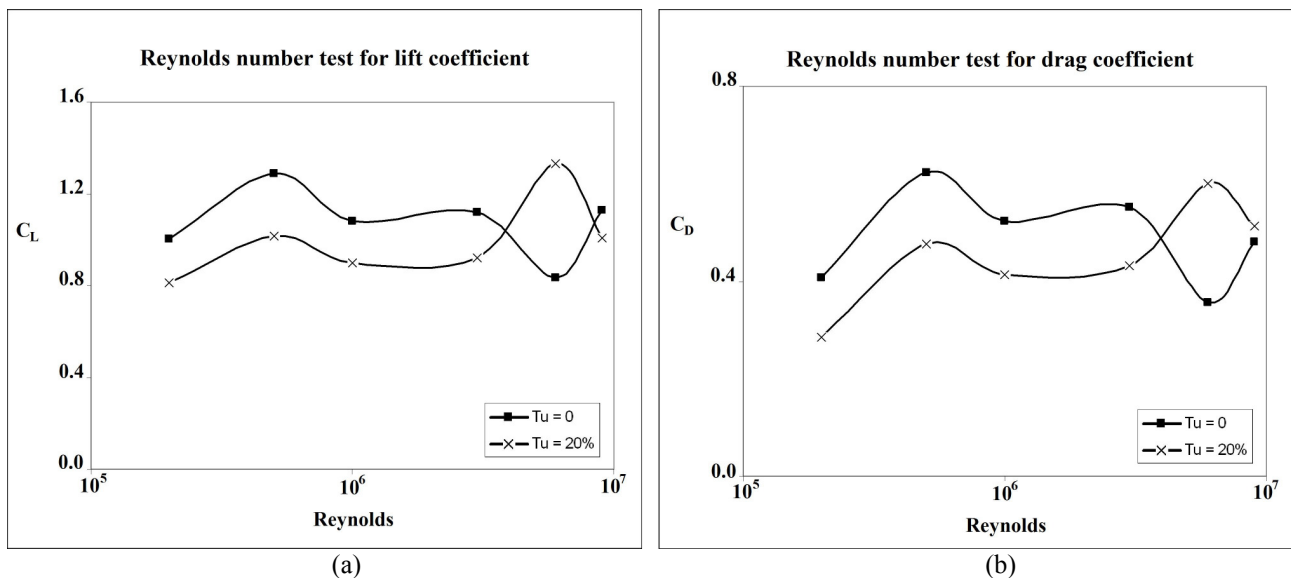


Figure 7. Reynolds number test for (a) lift and (b) drag coefficients.

The entire range of Reynolds number showed a similar dependency on turbulence intensity for both coefficients except for $Re\ 6 \times 10^6$, for which a reversal behavior was noticed. The reasons for this change might be simply numerical and are unknown by the authors. Based on the results, all the following simulations were performed for $Re\ 3 \times 10^6$, an intermediate value in the range considered and for which the results can also be compared with Abbott & von Doenhoff (1949).

5.2. Influence on lift

Figure 8 shows the comparison between the results obtained with simulations for the $c_l \times \alpha$ curves for both airfoils and the correspondent experimental data from Abbott & von Doenhoff (1949) for Reynolds 3×10^6 . A freestream turbulence intensity of 1% was used due to the unknown turbulence in the wind tunnel used in experiments.

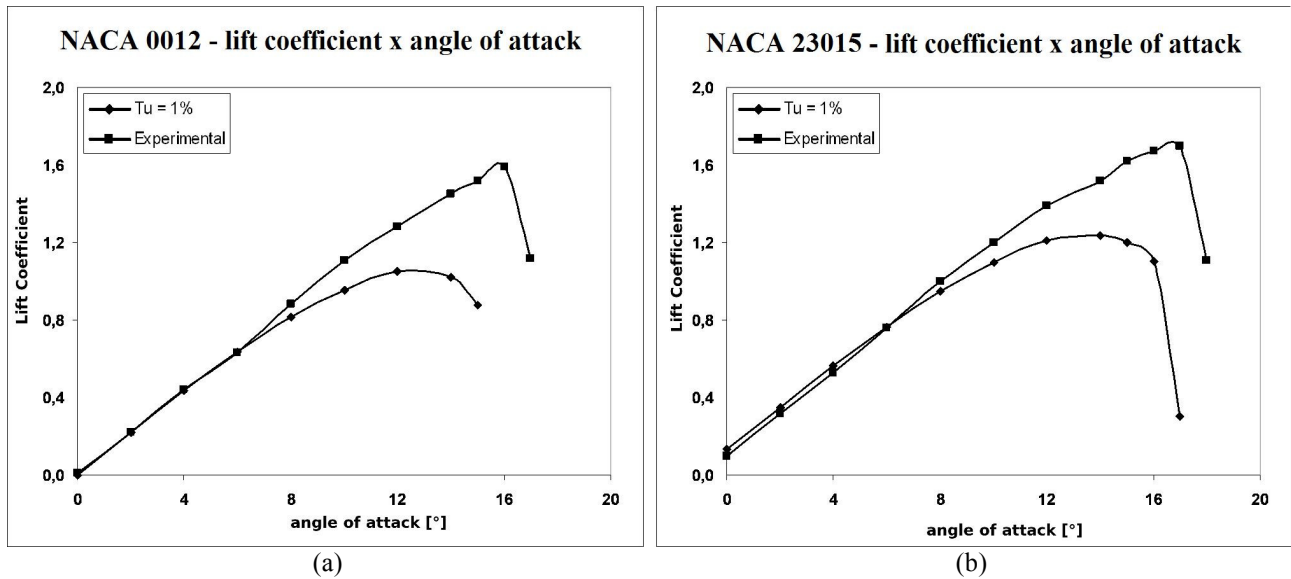


Figure 8. Comparison with experimental data for $c_L \times \alpha$ curves for (a) 0012 and (b) 23015 airfoils.

As one can see, the linear portions of both curves are very coherent with experimental results, but in the nonlinear regions large deviations exist. For both cases, the maximal lift coefficients are considerably lower than in the experiments and the stall occurs prematurely.

Next, a comparison between $c_L \times \alpha$ curves is presented for freestream turbulence intensities of 1%, 10% and 20%.

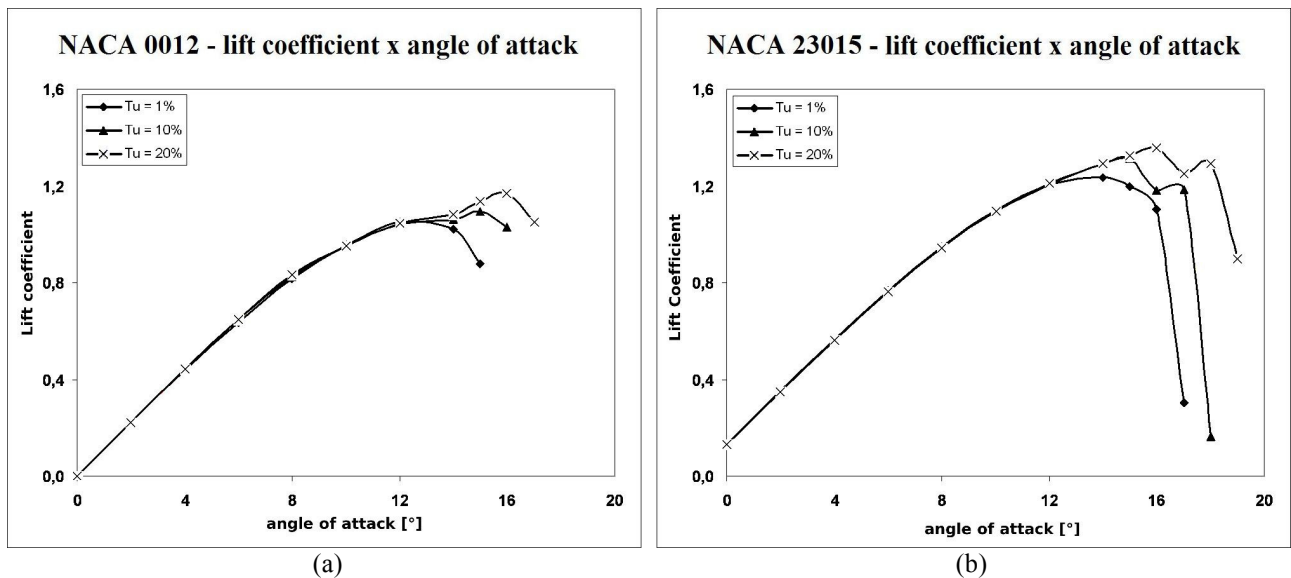


Figure 9. Comparison of $c_L \times \alpha$ curves for different turbulence intensities for (a) 0012 and (b) 23015 airfoils.

The plots show a high dependency of lift on turbulence intensities in the nonlinear region, suggesting a higher maximal lift coefficient and a delayed and smoother stall with the increase of freestream turbulence in both cases. In the linear region, no significant changes were observed.

5.3. Influence on drag

Figure 10 shows the drag polars for both NACA airfoils for the same three turbulence intensities.

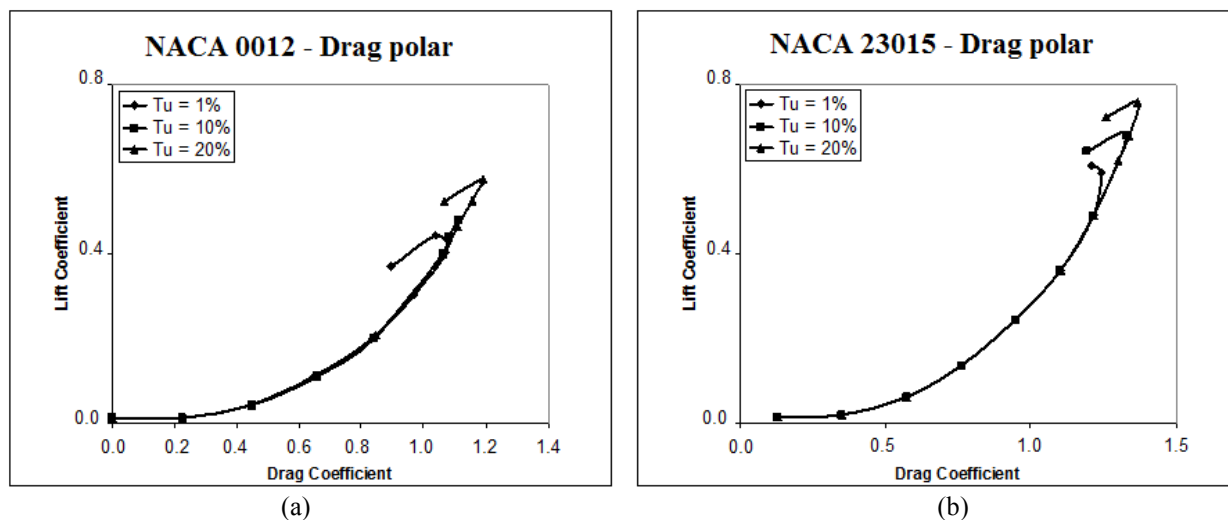


Figure 10 – Drag polars for different turbulence intensities for (a) 0012 and (b) 23015 airfoils.

The curves present no variations in drag with freestream turbulence intensity for low lift coefficients, what is an unexpected result. For high lift coefficients, differences in polar curves are noticed due to the changes in the stalling behavior presented previously.

6. CONCLUSION

The numerical simulation of external turbulent flows is a very challenging task and the difficulties extend from the definition of the domain size to the choice of an appropriate turbulence model. Each combination of geometry, angle of attack, Reynolds number and freestream turbulence intensity defines a singular problem that might require a specific mesh. Therefore, the mesh test performed for the NACA 0012 airfoil at 14° incidence with a Reynolds of 3×10^6 and with no freestream turbulence does not guarantee mesh-independent solutions for the other cases, which should be interpreted only as approximations. However, the high incidence used intends to amplify the participation of viscous phenomena and minimize the intrinsic errors.

Comparing the simulation results with the experimental data, one can notice that the linear region agrees well with experiments for both airfoils. A lower maximal lift coefficient and an early stall are not surprising incidents for two-dimensional turbulent aerospace flows using the SST model as suggested by Bigarella (2008). Therefore, the results for the nonlinear region are not conclusive.

In despite of the not relevant quantitative results, the freestream turbulence intensity seems to raise the maximal lift coefficient, also retarding and producing a smoother stall. This fact is due to the increased transport of momentum and, from this point of view, the external turbulence can be considered as advantageous to airfoils. The linear region remains unaltered independent on the magnitude of freestream turbulence.

The drag polars indicated no changes when submitted to different values of external turbulence. Additionally, very high drag is verified through the entire range of the curves, revealing a deficiency in the prediction of the boundary layer evolution. Both aspects suggest a completely turbulent boundary layer or an insignificant laminar portion.

7. REFERENCES

- Abbott, I.H. and Von Doenhoff, A. E., 1949, "Summary of Airfoil Data", NACA Report 824, 270 p.
- Bigarella, E.D.V. and Azevedo, J.L.F., 2008, "Modelagem de Turbulência para Aplicações Aeroespaciais", EPTT 2008, Brazil, pp. 536-617.
- Menter, F.R., 1992, "Influence of Freestream Values on $k-\omega$ Turbulence Model Predictions", AIAA Journal, Vol. 30, No. 6, pp. 1657-1659
- Menter, F.R., 1994, "Two-Equation Eddy Viscosity Turbulence Models for Engineering Applications", AIAA Journal, Vol. 32, No. 8, pp. 1598-1605.
- Schlichting, H., 2000, "Boundary Layer Theory", Ed. Springer, New York, United States of America, 801 p.
- Rezende, A.L.T., Sampaio, L.E.B. and Niekle, A.O., 2008, "Reynolds Avarage Navier-Stokes Simulation of Highly Anisotropic Turbulence Structures", EPTT 2008, pp. 41-49.

8. RESPONSIBILITY NOTICE

The authors are the only responsible for the printed material included in this paper.